Domingo Asensi, LR.; Pérez, P.; Aurell Piquer, MJ.; Sáez Cases, JA. (2012). Understanding the Bond Formation in Hetero Diels-Alder Reactions. An ELF Analysis of the Reaction of Nitroethylene with Dimethylvinylamine. Current Organic Chemistry. 16:2343-2351. doi:10.2174/138527212803520263.

Understanding the Bond Formation in Hetero-Diels-Alder Reactions. An ELF Analysis of the Reaction of Nitroethylene with Dimethylvinylamine.

Luis R. Domingo*[1], Patricia Pérez*[2], M. José Aurell[1] and José A. Sáez[3]

[1] Universidad de Valencia, Departamento de Química Orgánica,
Dr. Moliner 50, E-46100 Burjassot, Valencia, Spain.

[2] Universidad Andrés Bello, Facultad de Ciencias Exactas,
Departamento de Ciencias Químicas, Laboratorio de Química Teórica,
Av. República 275, 8370146 Santiago, Chile.

[3] Instituto de Tecnología Química UPV-CSIC, Universidad Politécnica de Valencia,
Camino de Vera s/n 46022 Valencia, Spain.

E-mails: p.perez@unab.cl and domingo@utopia.uv.es

Abstract

The bonding evolution in hetero-Diels-Alder (HDA) reactions has been studied by an ELF analysis of the electron reorganization along the HDA reaction between nitroethylene **6** and dimethylvinylamine (DMVA) **9** at the B3LYP/6-31G* level. This cycloaddition takes place along a two-stages one-step mechanism. In the first stage of the reaction, the C1-C6 bond is formed by coupling of two *pseudoradical* centers positioned at the most electrophilic carbon of nitroethylene **6** and the most nucleophilic center of DMVA **9**. In the second stage, the formation of the second O4-C7 bond takes place between a *pseudoradical* center positioned at the C7 carbon of DMVA and some electron-density provided by the lone pairs of the O4 oxygen. This behavior is in complete agreement with analyses of the local electrophilicity and nucleophilicity indices, and the spin density of the radical anion of nitroethylene **6** and of the radical cation of DMVA **9**. Finally, a relationship between the polar character of the reaction and the regioselectivity has been established.

Introduction

The Diels-Alder (DA) reaction is arguably one of the most powerful reactions in the arsenal of the synthetic organic chemist [1,2]. It permits the rapid construction of six-membered carbocycles from a 1,3-butadiene, the diene, and an ethylene derivative, the dienophile, with a high stereo- and regioselectivity. The diversity of substitution which may be present in the diene and the dienophile enables the DA reaction to be one of the most important synthetic organic reactions. The synthetic utility of this reaction does not arise only from the substitution in both the diene and the dienophile, but also from the exchange of one or more carbon atoms of the π system by a heteroatom such as O, N, S, P, etc. (see Chart 1). The corresponding DA reactions are called hetero-Diels-Alder (HDA) reactions, having a significant importance because they allow for the construction of six-membered heterocycles.

(please insert Chart 1)

Usually, DA reactions take place through an one-step mechanism. Only, in the singular cases in which the substitution allows for a stabilization of feasible biradical or zwitterionic intermediates, the reaction becomes stepwise. One-step mechanisms can take place through synchronous or asynchronous σ bond-formation processes.

Electron localization function [3-6] (ELF) analysis of bonding along the intrinsic reaction coordinate (IRC) of the DA reaction of cyclopentadiene (**1**, Cp) with ethylene (**2**), which is classified as a non-polar Diels-Alder (N-DA) reaction [7], indicates that this synchronous σ bond-formation process takes place according to the following pattern (see Figure 1) [8]: i) breaking of the three π bonds present in **1** and **2**; ii) formation of two *pseudodiradical* species; iii) formation of the two new σ bonds by coupling of two *pseudodiradical* species, and iv) formation of the new C-C π bond present in cycloadduct (CA) **3** at the end of the reaction. It is interesting to remark that

the transition state (TS) structure associated with this N-DA reaction is located at the end of phase i; consequently, the C-C bond formation has not started yet in the TS. This picture makes possible to rule out any concerted bond-breaking and bond-formation processes as proposed by the pericyclic model in which they would take place concurrently around a cyclic electron rearrangement.

(please insert Figure 1)

However N-DA reactions do not have any synthetic interest due to the drastic experimental conditions demanded as a consequence of the high activation energy associated with the formation of these *pseudodiradical* species [8]. The presence of electron-withdrawing substituents in the dienophile, such as 1,1-dicyanoethylene (**4**, DCE), favors DA reactions by lowering the activation energy [9]. The corresponding acceleration is related with the polar character of the reaction, allowing for the classification of polar Diels-Alder (P-DA) reactions [7]. This substitution breaks the symmetry of the dienophile, making the C–C σ bond formation asynchronous [9].

ELF bonding analysis along the P-DA reaction of Cp **1** with DCE **4** indicates that the bond formation takes place through a two-stages one-step mechanism. The two C-C σ bonds are formed according to the following pattern (see Figure 2) [10]: i) breaking of the three π systems in both Cp **1** and DCE **4**; ii) formation of the *pseudoradical* centers at the most nucleophilic center of Cp **1** and the most electrophilic center of DCE **4**; iii) formation of the first C-C σ bond by coupling of the electron-density accumulated at these *pseudoradical* carbons; iv) formation of the π system at the Cp framework and concentration of electron-density at the two carbon atoms to form two new *pseudoradical* centers; and v) formation of the second C-C σ bond by coupling of the electron-density accumulated at these carbons. In P-DA reactions the changes in electron-density are favored by the charge transfer (CT) which takes place from the

nucleophile, Cp **1**, to the electrophile, DCE **4**. This CT begins at an earlier step of the reaction, at *ca* 3.0 Å, and increases along the reaction until the formation of the first C-C σ bond is finished. Note that the CT at the asynchronous TS of this reaction, which is located at phase iii before forming the first C-C σ bond, is 0.28e. Thus, the observed acceleration in P-DA reactions with the increase of the CT can be related with the feasibility of formation of the corresponding zwitterionic *pseudodiradical* species involved in the C-C bond formation [10].

(please insert Figure 2)

In 1999, we studied the effects of the electron-releasing substitution on the dipolarophile in the HDA reactions of electrophilic nitroethylene **6** with three ethylenes of increasing nucleophilicity: propene **7**, methyl vinyl ether **8**, and dimethylvinylamine (DMVA) **9** (see Scheme 1) [11]. A good correlation between the acceleration of the reaction and the polar character of the TS was established. The polar character measured by the CT at the TS of the reaction no only accelerates the reaction but also increases the *endo* stereo and *ortho* regioselectivity [11].

(please insert Scheme 1)

We have recently studied the changes in bonding along N-DA [8] and P-DA [10] reactions given in Figures 1 and 2. Herein, we present an ELF analysis of the electron-reorganization along the most favorable *endo/ortho* reactive channel associated with the HDA reaction between nitroethylene **6** and DMVA **9**, which corresponds to the most P-DA reaction of the series given in Scheme 1 [11]. The purpose of this paper is to shed light on the electronic changes during HDA reactions, and to provide new insight into the answer this question: how does the C-O bond in HDA reactions take place, and which is the origin of the asynchronicity in bond-formation and regioselectivity?; in other words, the question is how electrons flow during the reaction?.

Computational Methods

DFT calculations were carried out using the B3LYP [12,13] exchange-correlation functionals, together with the standard 6-31G* basis set [14]. The optimizations were carried out using the Berny analytical gradient optimization method [15,16]. The stationary points were characterized by frequency calculations in order to verify that TSs have one and only one imaginary frequency. The IRC [17] paths were traced in order to check the energy profiles connecting each TS to the two associated minima of the proposed mechanism using the second order González-Schlegel integration method [18,19]. The electronic structures of stationary points were analyzed by the natural bond orbital (NBO) method [20,21] and by the ELF topological analysis, $\eta(\mathbf{r})$ [3-6]. The ELF study was performed with the TopMod program [22] using the corresponding monodeterminantal wavefunctions of the selected structures of the IRC. All calculations were carried out with the Gaussian 03 suite of programs [23].

The global electrophilicity index [24], ω, is given by the following simple expression [24], $\omega = (\mu^2 / 2\eta)$, in terms of the electronic chemical potential μ and the chemical hardness η. Both quantities may be approached in terms of the one electron energies of the frontier molecular orbital HOMO and LUMO, ε_H and ε_L, as $\mu \approx (\varepsilon_H + \varepsilon_L)/2$ and $\eta \approx (\varepsilon_L - \varepsilon_H)$, respectively [25,26]. Recently, we have introduced an empirical (relative) nucleophilicity index [27,28], N, based on the HOMO energies obtained within the Kohn-Sham scheme [29], and defined as $N = E_{HOMO}(Nu) - E_{HOMO}(TCE)$. The nucleophilicity is referred to TCE, because it presents the lowest HOMO energy in a large series of molecules already investigated in the context of polar cycloadditions. This choice allows us conveniently to handle a nucleophilicity scale of

positive values [28]. Local electrophilicity indices [30], ω_k, and the local nucleophilicity indices [31], N_k, were evaluated using the following expressions: $\omega_k = \omega f_k^+$ and $N_k = N f_k^-$, where f_k^+ and f_k^- are the Fukui functions for nucleophilic and electrophilic attacks, respectively [32].

Results and Discussion

This study is divided into four parts: i) first, an analysis of the stationary points involved in the *ortho* and *meta* regioisomeric channels associated with the *endo* approach of DMVA **9** to nitroethylene **6** is performed; ii) then, an analysis of the reagents based on the DFT reactivity indices will be completed in order to state the reactivity and regioselectivity in this HDA reaction; iii) thereafter, a complete ELF analysis along the most favorable *endo*/*ortho* reactive channel associated with the HDA reaction between nitroethylene **6** and DMVA **9** will be performed to analyze the changes in bonding; iv) finally, an analysis of the factors controlling the asynchronicity in bond-formation and regioselectivity in this HDA reaction will be carried out.

*1) Analysis of the stationary points involved in the two regioisomeric channels associated with the endo approach of dimethylvinylamine **9** to nitroethylene **6**.*

Analysis of the stationary points involved in the HDA reaction between nitroethylene **6** and DMVA **9** indicates that this cycloaddition takes place via a one-step mechanism through a high asynchronous TS. Details of energies and structures of the stationary points are not discussed here. A detailed discussion is found in ref 7. The most relevant features of the *endo* regioisomeric **TSno** and **TSnm** are given in Figure 3.

(please insert Figure 3)

Some relevant characteristics of these TSs must be pointed out: i) the most favorable *ortho* **TSno** presents a low activation energy, 4.7 kcal/mol, as a consequence of the strong electrophilic character of nitroethylene **6** and the strong nucleophilic character of DMVA **9** (see later). Note that the N-DA reaction between Cp **1** and ethylene **2** presents a very high activation energy: 19.9 kcal/mol [8]; ii) the regioisomeric *meta* **TSnm** presents a very high activation energy, 29.2 kcal/mol, i.e., **TSnm** is 24.5 kcal/mol higher in energy than **TSno**; iii) both regioisomeric TSs present a high asynchronicity: Δl(**TSno**) = 0.89 Å and Δl(**TSnm**) = 1.29 Å, where $\Delta l = (d1 - d2)$ (d1 and d2 are the lengths of the two forming bonds); iv) while the bond-formation begins at the most favorable *ortho* **TSno** at the C1 carbon atom of nitroethylene **6**, at the most unfavorable regioisomeric *meta* **TSnm** it begins at the O4 oxygen; and v) the CT at the most unfavorable *meta* **TSnm**, 0.50e, is higher than that at the most favorable *ortho* **TSno**, 0.41e.

2) Analysis based on DFT reactivity indices.

Studies carried out on cycloaddition reactions have shown that the indices defined within the conceptual DFT [33,34] are powerful tools for analyzing the reactivity and the regioselectivity in polar reactions. The static global properties, namely electronic chemical potential μ, chemical hardness η, global electrophilicity ω, and global nucleophilicity, N, for nitroethylene **6** and DMVA **9** are displayed in Table 1, while their local properties are presented in Table 2.

Table 1. Electronic chemical potential μ, chemical hardness η, global electrophilicity ω, and global nucleophilicity, N, in eV, for nitroethylene **6** and DMVA **9**.

	μ	η	ω	N
DCE **4**	-5.64	5.65	2.82	0.65
nitroethylene **6**	-5.33	5.45	2.61	1.07
Cp **1**	-3.01	5.49	0.83	3.37
ethylene **2**	-3.37	7.77	0.73	1.86
propene **7**	-3.01	7.57	0.60	2.32
methyl vinyl ether **8**	-2.43	6.98	0.42	3.20
DMVA **9**	-1.87	6.50	0.27	3.99

The electronic chemical potential of nitroethylene **6**, μ = -5.33 eV, is below the electronic chemical potential of DMVA **9**, μ = -1.87 eV, thereby indicating that in a polar process, the net CT will take place from DMVA **9** to the electron-deficient nitroethylene **6**, in clear agreement with the CT observed at the TSs.

Nitroethylene **6** has a high electrophilicity index, ω = 2.61 eV, being classified as a strong electrophile within the electrophilicity scale [35]. Nitroethylene **6**, is one of the most electrophilic species of the monosubstituted ethylene series. On the other hand, nitroethylene **6** presents a nucleophilicity index of N = 1.07 eV, being classified as a marginal nucleophile [36].

DMVA **9** has a very low electrophilicity index [24], ω= 0.27 eV, being classified as a marginal electrophile within the electrophilicity scale. On the other hand, **9** presents a very high nucleophilicity index [27,28], N = 3.99 eV, being classified as a strong nucleophile. Note that DMVA **9** is the most nucleophilic dienophile of Scheme 1 (see Table 1). Therefore, the electrophilicity difference between the heterodiene **6** and the electron-rich dienophile **9**, $\Delta\omega$ = 2.34 eV, which has been proposed as a measure of the polar character of DA reactions involving simple molecules [35], indicates that this reaction will have a large polar character, in clear agreement with the CT analysis

performed at **TSno**. Note that the P-DA reaction between Cp **1** with DCE **4** presents a lower $\Delta\omega$, 1.99 eV. The lower polar character of this reaction is in clear agreement with the lower CT found at the corresponding TS, 0.28e, and the larger activation energy, 9.3 kcal/mol [35].

The local electrophilicity [30], ω_k, and nucleophilicity [31], N_k, indices can be used to measure the distribution of the global electrophilicity and nucleophilicity at the different atomic sites of a molecule, and thus state the local reactivity. Along a polar reaction involving asymmetric reagents, the most favorable reactive channel is that involving the initial interaction between the most electrophilic and nucleophilic center of both reagents.

Table 2. Local electrophilicity ω_k, and local nucleophilicity, N_k, in eV, for nitroethylene **6** and DMVA **9**.

.

nitroethylene **6**	ω_k	DMVA **9**	N_k
C1	0.73	C6	1.64
C2	0.20	C7	0.37
N3	0.61	N8	1.54
O4	0.57		
O5	0.50		

Analysis of the local electrophilicity ω_k in the asymmetric nitroethylene **6** shows that the most electrophilic center of this molecule corresponds to the C1 carbon, ω_{C1} = 0.73 eV, although the nitrogen and the oxygen atoms belonging to the NO_2 group also present a strong electrophilic activation, ω_{N3} = 0.61 eV, ω_{O4} = 0.57 eV and ω_{O5} = 0.50 eV. The most nucleophilic activated centers of DMVA **9** are the C6 carbon, N_{C6} = 1.64 eV, and the N8 nitrogen, N_{N8} = 1.54 eV. Therefore, the most favorable reactive channels will be those involving the participation of the C1 carbon of nitroethylene **6**

and the C6 carbon of DMVA **9**, in clear agreement with the total regioselectivity observed.

*3) ELF bonding analysis along the IRC path of the HDA reaction between nitroethylene **6** and DMVA **9**.*

Recent theoretical studies have shown that the topological analysis of the ELF along the reaction path associated with a cycloaddition is a valuable tool for understanding the bonding changes along the reaction path [8,10,37-43]. Consequently, a topology analysis of the ELF along the IRC of the most favorable *endo/ortho* channel associated with the HDA reaction between nitroethylene **6** and DMVA **9** was performed in order to understand the asynchronous bond-formation in this HDA reaction. The *N* populations of the more relevant ELF valence basins in different phases along the IRC are listed in Table 3. A schematic picture of the bonding changes along the different phases involved in this HDA reaction is given in Figure 4, while the attractor positions and atom numbering for the most relevant points are shown in Figure 5.

Table 3. Valence basin populations *N* calculated from the ELF of some selected points associated with the asynchronous formation of the C1-C6 and O4-C7 σ bonds along the HDA reaction between nitroethylene **6** and DMVA **9**. The CT along the IRC is also included.

Phase	**6** & **9**	I	II	III	IV	V **TSno**	VI	VII	VIII	IX	X **CAno**
d1 = d(C1,C6)		3.53	2.54	2.20	2.17	2.04	1.98	1.57	1.57	1.56	1.54
d2 = d(O4,C7)		3.45	3.08	2.97	2.97	2.94	2.92	1.95	1.91	1.78	1.44
BO(C1,C6)		0.02	0.14	0.33	0.35	0.47	0.53	0.96	0.96	0.97	1.00
BO(O4,C7)		0.00	0.02	0.03	0.03	0.04	0.05	0.44	0.47	0.57	0.82
CT (ELF)		0.01	0.19	0.30	0.31	0.35	0.62	0.61	0.62	0.60	0.29
CT (BO)		0.04	0.17	0.32	0.33	0.41	0.45	0.53	0.52	0.47	0.37
V(C1,C2)	1.77	1.75	1.73	3.51	3.55	2.79	2.69	2.01	2.02	2.01	2.01
V'(C1,C2)	1.78	1.79	1.78								
V(C2,N3)	2.79	2.80	2.94	3.06	3.02	3.12	3.17	3.63	3.66	3.97	4.07
V(N3,O4)	1.73	1.72	1.59	1.57	1.58	1.53	1.55	1.47	1.47	1.46	1.53
V(N3,O5)	1.70	1.70	1.65	1.58	1.57	1.56	1.52	1.23	1.21	1.17	1.01
V(O4)	2.78	2.86	2.86	2.87	2.90	2.92	2.93	2.91	2.94	2.94	2.71
V'(O4)	2.94	2.92	2.95	2.99	2.99	2.98	3.00	3.08	3.10	3.09	2.56
V(O5)	2.84	2.88	2.90	2.90	2.93	2.92	2.94	2.93	2.90	2.87	2.74
V'(O5)	2.84	2.88	2.92	2.93	2.92	2.97	2.97	3.03	3.07	3.05	3.09
V(C6,C7)	1.87	1.79	3.48	3.34	2.90	2.70	2.61	2.13	2.12	2.08	2.00
V'(C6,C7)	1.87	1.86									
V(C7,N8)	2.35	2.43	2.01	2.20	2.94	2.93	2.98	2.64	2.53	2.40	2.04
V(N8)	1.68	1.70	1.15	1.09	1.08	0.99	0.95	1.57	1.62	1.77	2.09
V'(N8)			0.95	0.74							
V(C2)						0.55	0.61	0.52	0.49	0.47	0.35
V'(C2)								0.26	0.26		
V(C1)						0.20					
V(C6)					0.45	0.61					
V(C7)									0.07	0.21	
V(C1,C6)							0.95	1.74	1.74	1.77	1.82
V(O4,C7)											1.13

(please insert Figure 4)

(please insert Figure 5)

ELF analysis of nitroethylene **6** shows two disynaptic basins V(C1,C2) and V'(C1,C2) associated with the C1-C2 double bond, whose electronic populations integrate 1.77e and 1.78e, one disynaptic basin V(C2,N3), integrating 2.79e, and two disynaptic basins V(N3,O4) and V(N3,O5), integrating 1.73e and 1.70e. Finally, nitroethylene **6** also shows four monosynaptic basins V(O4), V'(O4), V(O5) and V'(O5), each one integrating *ca* 2.8e, associated with the lone pairs present at the O4

and O5 oxygen atoms. On the other hand, DMVA **9** presents two disynaptic basins, V(C6,C7) and V'(C6,C7), associated with the C6-C7 double bond, whose electronic populations integrate 1.87e each one, one disynaptic basin V(C7,N8), integrating 2.35e, and one monosynaptic basin V(N8), associated with the lone pair at the N8 nitrogen, whose electronic population integrates 1.68e.

Analysis of ELF basin populations along the IRC of the HDA reaction between nitroethylene **6** and DMVA **9** allows for the characterization of ten phases (see Table 3 and Figure 4). Phase I, d1 = d(C1-C6) > 3.53 Å and d2 = d(O4-C7) > 3.45 Å, shows the ELF picture of attractors of the separated reagents. Whereas the two reactants approach each other along the short phase II, 3.53 > d1 > 2.54 Å and 3.45 > d2 > 3.08 Å, the two disynaptic basins associated with the C6-C7 double bond of vinylamine moiety merge into the disynaptic basin V(C6,C7), whose electronic population integrates 3.48e. While the disynaptic basin V(C7,N8) experiences a strong reduction in electron-density reaching 2.01e, the monosynaptic basin V(N8) splits into two monosynaptic basins, V(N8) and V'(N8), integrating 1.15 and 0.95e. An appreciable CT takes place from DMVA **9** to nitroethylene **6**, 0.19e (0.17e BO) in this early phase. In phase III, 2.54 > d1 > 2.20 Å and 3.08 > d2 > 2.97 Å, the two disynaptic basins associated with the C1-C2 double bond of the nitroethylene moiety merge into one disynaptic basin V(C1,C2), whose electronic population integrates 3.51e. At the end of this phase, an appreciable CT takes place, 0.30e (0.32e BO).

The most relevant changes of the cycloaddition occur in phases IV to VI located in a narrow region of the IRC. In the short phase IV, 2.20 > d1 > 2.17 Å and 2.97 > d2 > 2.97 Å, some relevant changes take place in the vinylamine moiety. While a new monosynaptic basin V(C6), integrating 0.45e, appears at the terminal C6 carbon of the vinylamine moiety, the disynaptic basin V(C6,C7) experiences a strong reduction in

electron-density reaching 2.90e (see Figure 5). Simultaneously, two monosynaptic basins V(N8) and V'(N8) merge into the former, integrating 1.08e.

In the short phase V, 2.17 > d1 > 2.04 Å and 2.97 > d2 > 2.94 Å, while the monosynaptic basin V(C6) reaches 0.61e, a new monosynaptic basin V(C1), integrating 0.20e, appears at the terminal C1 carbon of the nitroethylene moiety (see Figure 5). Interestingly, an unexpected monosynaptic basin V(C2), integrating 0.55e, appears at the C2 carbon of nitroethylene. This basin remains even in the final **CAno**. Note that this monosynaptic basin V(C2) appears also in phase VI in the P-DA reaction between Cp **1** and DCE **4**; however, in this reaction it disappears with the formation of the second C-C bond at the end of the cycloaddition [10]. The disynaptic basin V(C1,C2) experiences a strong reduction in electron-density reaching 2.79e. This change can be related to the formation of the two new monosynaptic basins V(C1) and V(C2), the former required for the formation of the new C1-C6 bond. Note that the total population of the monosynaptic basins V(C1) and V(C2), *ca* 0.8e, agrees with the loss of the population in the disynaptic basin V(C1,C2), 0.8e. In this phase, the TS of the reaction is located at d1= 2.044 and d2= 2.938 Å, which presents a large CT, 0.35e (0.41e BO). In the short phase VI, 2.04 > d1 > 1.98 Å and 2.94 > d2 > 2.92 Å, another relevant changes along the IRC take place. The two monosynaptic basins V(C1) and V(C6), positioned at the terminal C1 and C6 carbons of the reagents, merge into a new disynaptic basin V(C1,C6), integrating 0.95e. These changes are associated with the formation of the first C1-C6 σ bond, at a distance of 2.00 Å. The population of this basin is increased along the IRC until reaching the formation of **CAno**. At this phase, the monosynaptic basin V(C2) reaches 0.61e, whereas the population of the disynaptic basin V(C1,C2) is decreased to 2.69e. Along this phase a large amount of CT takes place, 0.62e (0.45e BO).

Phase VII, 1.98 > d1 > 1.57 Å and 2.92 > d2 > 1.95 Å, constitutes a wide space of the IRC, in which a second monosynaptic basin is created at C2, V'(C2), integrating 0.26e. Interestingly, while the electron-density of the disynaptic basin V(C1,C6) associated to the new C1-C6 σ bond is increased by 0.79e, the electron-density of the disynaptic basin V(C6,C7) is depopulated by 0.48e (see Figure 5). Taking into account that the population of the disynaptic basin V(C1,C6) in **CAno** is 1.82e, it can be considered that the formation of C1-C6 has been completed by 96%. In this step, at d1= 1.62 and d2= 2.45 Å, the maximum CT along the IRC takes place, 0.74e. Phase VII divides the one-step mechanism of the cycloaddition in the two-stages; while the C1-C6 σ bond is practically already formed, the formation of the O4-C7 bond has not yet started. At the end of this phase, the CT begins to decrease as a consequence of a retro-donation process.

In the short phase VIII, 1.57 > d1 > 1.57 Å and 1.95 > d2 > 1.91 Å, a new monosynaptic basin at C7, namely V(C7), with a minimal electronic population of 0.07e has begun to appear. Along this phase, the population of the disynaptic basin V(C1,C6) reaches 1.74e, indicating that the C1-C6 σ bond is practically already formed. Finally, the monosynaptic basins V(O4) and V'(O4), and V(O5) and V'(O5) associated with the lone pairs of the O4 and O5 oxygen atoms, reach 6.04e and 5.97e, respectively. Note that in nitroethylene **6**, the total population of these monosynaptic basins is 5.72e and 5.68e, respectively. Consequently, a large amount of the electron-density transferred to the nitroethylene is concentrated at the terminal O4 and O5 oxygen atoms.

In phase IX, 1.57 > d1 > 1.56 Å and 1.91 > d2 > 1.78 Å, the population of the monosynaptic basin V(C7) reaches 0.21e, while the population of the disynaptic basins V(C7,N8) is decreased to 2.40e (see Figure 5). Simultaneously, while the population of the two monosynaptic basins present in C2 decreases by a total amount of 0.28e, the

population of the disynaptic basin V(C2,N3) increases in 0.31e to 3.97e. These changes indicate that part of the electron-density belonging to the monosynaptic basins V(C2) and V'(C2) present in the previous phase is absorbed by the disynaptic basin V(C2,N3). At the beginning of phase X, 1.56 > d1 > 1.54 Å and 1.78 > d2 > 1.44 Å, the monosynaptic basin V(C7) merges into a new disynaptic basin V(O4,C7), which integrates 0.79e. Note that the formation of this disynaptic basin, which is associated with the formation of the second O4-C7 σ bond, demands together with the annihilation of the monosynaptic basin V(C7) a depopulation of 0.50e of the monosynaptic basins V(O4) and V'(O4). The low population of the disynaptic basin V(O4,C7) at **CAno**, 1.13e, accounts for a strongly polarized C4-C7 σ bond.

Some significant conclusions can be drawn from this ELF bonding analysis: i) this HDA reaction involving asymmetric reagents takes place via a two-stages one-step mechanism with a very high polar character. Formation of the first C1-C6 bond takes place in the first stage of the reaction. The corresponding changes in bonding to reach the complete formation of the C1-C6 σ bond cover a wide extension of the IRC, phases I to VII. On the other hand, formation of the second O4-C7 bond takes place at the end of the IRC, phase X; ii) The most noticeable behavior of **TSno**, which is located in phase V, is the presence of a monosynaptic basin V(C1) at the C1 carbon of nitroethylene and a monosynaptic basin V(C6) at the C6 carbon of DMVA; iii) the C1-C6 bond formation begins at in phase VI by merging the two monosynaptic basins positioned at the terminal C1 and C6 carbons, d(C1-C6) = 2.04 Å. This distance is very close to that found in the formation of the first C-C bond in the P-DA reaction between Cp **1** and DCE **4**: 1.99 Å [10]; iv) the O4-C7 bond formation, which takes place at d(O4-C7) = 1.78 Å, involves the monosynaptic basin V(7) and some of the electron-density belonging to one monosynaptic basin of the O4 oxygen. This fact is similar to

that found in the C-O bond formation in the 1,3-dipolar cycloaddition between a carbonyl ylide as dipole and the C=O of a 1,2-benzoquinone as dipolarophile [44]; v) analyses of the CT along the cycloaddition based on the NBO and ELF show a similar pattern. The CT begins in an earlier phase of the reaction from the nucleophile to the electrophile, reaching an amount of 0.62e (0.52e NBO) at the end of phase VIII. This CT process is associated with the formation of the first C1-C6 σ bond. After passing phase VIII, the CT decreases as a consequence of a retro-donating process associated with the formation of the second O4-C7 σ bond.

*4) Factors controlling the asynchronicity in bond formation and the regioselectivity in the HDA reaction between nitroethylene **6** and DMVA **9**.*

What is the origin of the asynchronicity in bond formation and the regioselectivity in this HDA reaction? ELF analysis along the most favourable *endo/ortho* reaction path associated with the HDA reaction between nitroethylene **6** and DMVA **9** shows an asynchronous C–C and C–O bond formation. Points of ELF belonging to phase V of this HDA reaction are similar to those found at phase V of the IRC of the P-DA reaction between Cp **1** and DCE **4** (see Figure 2 in reference 6). These points, which are characterized as *zwitterionic pseudodiradical* species [10], present two monosynaptic basins at C1 and C6 carbons of nitroethylene **6** and DMVA **9**, respectively. Note that these centers correspond to the most electrophilic and the most nucleophilic centers of these molecules as indicated by the local electrophilicity ω_k and local nucleophilicity N_k indices. We have recently suggested that some of the electron-density that integrates these monosynaptic basins comes from the CT process [10].

In the extreme case of transferring an amount of an electron density equivalent to one electron, nitroethylene **6** becomes a radical anion, and DMVA **9** becomes a radical cation. Analysis of the atomic spin density at the radical anion of nitroethylene **6** indicates that the spin density is mainly located at the C1 carbon, 0.49e, while that at the radical cation of DMVA **9** is located at the C6 carbon atom, 0.69e (see Figure 6). Consequently, the asymmetric distribution of electron-density in the nitroethylene and the DMVA moieties, achieved through the CT process along the polar cycloaddition is responsible for the formation of the C1 and C6 monosynaptic basins along the most favourable *ortho* pathways, and thus for the asynchronous bond formation.

(please insert Figure 6)

Accordingly, it appears that along a polar cycloaddition, the CT that takes place from the nucleophile towards the electrophile favours the electron-reorganization required to reach the formation of the monosynaptic basins in both the nucleophile and the electrophile. Then, the most favourable regioisomeric channel is that involving the bond formation between these *pseudoradical* centers. Thus, the asymmetric formation of these *pseudoradical* centers in the two reagents is responsible for the regioselectivity observed in P-DA reactions.

In spite of the few cases given in Scheme 1, a very good correlation between the CT at the most favourable *endo/ortho* TS and the regioselectivity measured by $\Delta\Delta E_{(TSm-TSo)}$ is found (see Figure 7a). In this series, the increase of regioselectivity can be also related to the nucleophilic character of the dienophile which increases in the order: propene **7** (N = 2.32 eV) < methyl vinyl ether **8** (N = 3.20 eV) < DMVA **9** (N = 3.99

eV) (see Figure 7b and Table 1). Therefore, a good relationship between the polar character of these HDA reactions and the regioselectivity can be established.

(please insert Figure 7)

Conclusions

The bonding evolution in HDA reactions has been studied by an ELF analysis of the electron reorganization along the HDA reaction between nitroethylene **6** and DMVA **9** at the B3LYP/6-31G* level. This reaction takes place along a two-stages one-step mechanism (see Figure 8). In the first stage of the reaction, the C1-C6 bond is formed by coupling of two *pseudodiradical* centers positioned in the most electrophilic carbon of nitroethylene **6**, the C1 carbon, and the most nucleophilic center of DMVA **9**, the C6 carbon (see bonding changes between phases V and VI in Figure 8). These *pseudodiradical* centers appear to be reached by the CT that takes place along the approach of the nucleophile to the electrophile, which reaches a maximum value with the formation of the first C-C bond (see the increase of CT between phases V and VI in Figure 8). This behavior is in complete agreement with the analysis of spin density of the radical anion of nitroethylene **6** and that of the radical cation of DMVA **9**.

In the second stage of the reaction the formation of the second O4-C7 bond between the *pseudoradical* center positioned at the C7 carbon of DMVA and some electron-density provided by the lone pairs of the O4 oxygen takes place (see bonding changes between phases IX and X in Figure 8). Along the O4-C7 bond formation, which occurs at the end of the cycloaddition, a retro-donation takes place from the nitro O4 oxygen (see the decrease of CT between phases IX and X in Figure 8).

The electron-reorganization at the zwitterionic *pseudoradical* species generated by the CT process along these polar reactions, which is similar to that shown by the radical anion of the electrophile and the radical cation of the nucleophile, accounts for the regioselectivity in P-DA reactions involving asymmetric electrophilic and

nucleophilic species. The most favorable regioisomeric channels are those associated with the most favorable C-to-C coupling at the zwitterionic *pseudoradical* species.

(please insert Figure 8)

Acknowledgment. We are grateful to the Spanish Government (project CTQ2009-11027/BQU), and the Fondecyt project No. 1100278. Professor Domingo also thanks Fondecyt by support through the Cooperación Internacional.

References

[1] Carruthers, W. *Some Modern Methods of Organic Synthesis*, Cambridge University Press, Cambridge, **1978**.

[2] Carruthers, W. *Cycloaddition Reactions in Organic Synthesis*, Pergamon, Oxford, **1990**.

[3] Savin, A.; Becke, A. D.; Flad, J.; Nesper, R.; Preuss, H.; Vonschnering, H. G. A new look at electron localization. *Angew. Chem. Int. Ed.*, **1991**, *30*, 409.

[4] Savin, A.; Silvi, B.; Colonna, F. Topological analysis of the electron localization function applied to delocalized bonds. *Can. J. Chem.*, **1996**, *74*, 1088.

[5] Savin A.; Nesper, R.; Wengert, S.; Fassler, T. F. ELF: The electron localization function. *Angew. Chem., Int. Ed. Engl.*, **1997**, *36*, 1809.

[6] Silvi, B. The synaptic order: A key concept to understand multicenter bonding. *J. Mol. Struct.*, **2002**, *614*, 3.

[7] Domingo, L. R.; Saez, J. A. Understanding the mechanism of polar Diels-Alder reactions. *Org. Biomol. Chem.*, **2009**, *7*, 3576.

[8] Domingo, L. R.; Chamorro, E.; Perez, P. Understanding the mechanism of non-polar Diels-Alder reactions. A comparative ELF analysis of concerted and stepwise diradical mechanisms. *Org. Biomol. Chem.*, **2010**, *8*, 5495.

[9] Domingo, L. R.; Aurell, M. J.; Perez, P.; Contreras, R. Quantitative Characterization of the Local Electrophilicity of Organic Molecules.

Understanding the Regioselectivity on Diels−Alder Reactions. *J. Org. Chem.*, **2003**, *68*, 3884.

[10] Domingo, L. R.; Perez, P.; Saez, J. A. Origin of the synchronicity in bond formation in polar Diels-Alder reactions: an ELF analysis of the reaction between cyclopentadiene and tetracyanoethylene. *Org. Biomol. Chem.*, **2012**, *10*, 3841.

[11] Domingo, L. R.; Arno, M.; Andres, J. Influence of reactant polarity on the course of the inverse-electron-demand Diels-Alder reaction. A DFT study of regio- and stereoselectivity, presence of Lewis acid catalyst, and inclusion of solvent effects in the reaction between nitroethene and substituted ethenes. *J. Org. Chem.*, **1999**, *64*, 5867.

[12] Becke, A. D. Density-functional thermochemistry. III. The role of exact exchange. *J. Chem. Phys.*, **1993**, *98*, 5648.

[13] Lee, C.; Yang, W.; Parr, R. G. Development of the colle-salvetti conelation energy formula into a functional of the electron density. *Phys. Rev. B*, **1988**, *37*, 785.

[14] Hehre, W. J.; Radom, L.; Schleyer, P. v. R.; Pople, J. A. *Ab initio Molecular Orbital Theory*, Wiley, New York, **1986**.

[15] Schlegel, H. B. Optimization of equilibrium geometries and transition structures. *J. Comput. Chem.*, **1982**, *3*, 214.

[16] Schlegel, H. B. *"Geometry Optimization on Potential Energy Surface," in Modern Electronic Structure Theory.* Yarkony D.R ed.: World Scientific Publishing: Singapore, 1994.

[17] Fukui, K. A formulation of reaction coordinate. *J. Phys. Chem.*, **1970**, *74*, 4161.

[18] González, C.; Schlegel, H. B. Reaction path following in mass-weighted internal coordinates. *J. Phys. Chem.* **1990**, *94*, 5523.

[19] González, C.; Schlegel, H. B. Improved algorithms for reaction path following: Higher-order implicit algorithms. *J. Chem. Phys.*, **1991**, *95*, 5853.

[20] Reed, A. E.; Weinstock, R. B; Weinhold, F. Natural population analysis. *J. Chem. Phys.*, **1985**, *83*, 735.

[21] Reed, A. E.; Curtiss, L. A.; Weinhold, F. Intermolecular interactions from a natural bond orbital, donor-acceptor viewpoint. *Chem. Rev.*, **1988**, *88*, 899.

[22] Noury, S.; Krokidis, X.; Fuster, F.; Silvi, B. Computational tools for the electron localization function topological analysis. *Comput. Chem.*, **1999**, *23*, 597.

[23] Frisch, M. J.; Trucks, G. W.; Schlegel, H. B.; Scuseria, G. E.; Robb, M. A.; Cheeseman, J. R.; Montgomery, J. J. A.; Vreven, T.; Kudin, K. N.; Burant, J. C.; Millam, J. M.; Iyengar, S. S.; Tomasi, J.; Barone, V.; Mennucci, B.; Cossi, M.; Scalmani, G.; Rega, N.; Petersson, G. A.; Nakatsuji, H.; Hada, M.; Ehara, M.; Toyota, K.; Fukuda, R.; Hasegawa, J.; Ishida, M.; Nakajima, T.; Honda, Y.; Kitao, O.; Nakai, H.; Klene, M.; Li, X.; Knox, J. E.; Hratchian, H. P.; Cross, J. B.; Adamo, C.; Jaramillo, J.; Gomperts, R.; Stratmann, R. E.; Yazyev, O.; Austin, A. J.; Cammi, R.; Pomelli, Ochterski, C.J. W.; Ayala, P. Y.; Morokuma, K.; Voth, G. A.; Salvador, P.; Dannenberg, J. J.;Zakrzewski, V. G; Dapprich, S.; Daniels, A. D.; Strain, M. C.; Farkas, O.; Malick, D. K.; Rabuck, A. D.; Raghavachari, K.; Foresman, J. B.; Ortiz, J. V.; Cui, Q.; Baboul, A. G.; Clifford, S.; Cioslowski, J.; Stefanov, B. B.; Liu, G.; Liashenko, A.; Piskorz, P.; Komaromi, I.; Martin, R. L.; Fox, D. J.; Keith, T.; Al-Laham, M. A.; Peng, C. Y.; Nanayakkara, A.; Challacombe, M.; Gill, P. M. W.; Johnson, B.; Chen, W.; Wong, M. W.; Gonzalez, C.; Pople J. A. *Gaussian03*, **2004**.

[24] Parr, R. G.; von Szentpaly, L.; Liu, S. Electrophilicity index. *J. Am. Chem. Soc.*, **1999**, *121*, 1922.

[25] Parr, R. G.; Pearson, R. G. Absolute hardness: companion parameter to absolute electronegativity. *J. Am. Chem. Soc.*, **1983**, *105*, 7512.

[26] Parr, R. G.; Yang, W. *Density Functional Theory of Atoms and Molecules*, Oxford University Press, New York, **1989**.

[27] Domingo, L. R.; Chamorro, E.; Perez, P. Understanding the reactivity of captodative ethylenes in polar cycloaddition reactions. A theoretical study. *J. Org. Chem.*, **2008**, *73*, 4615.

[28] Domingo, L. R.; Perez, P. The nucleophilicity N index in organic chemistry. *Org. Biomol. Chem.*, **2011**, *9*, 7168.

[29] Kohn, W.; Sham, L. Self-consistent equations including exchange and correlation effects. J. *Phys. Rev.*, **1965**, *140*, 1133.

[30] Domingo, L. R.; Aurell, M. J.; Perez, P.; Contreras, R. Quantitative characterization of the local electrophilicity of organic molecules. Understanding the regioselectivity on Diels-Alder reactions. *J. Phys. Chem., A,* **2002**, *106*, 6871.

[31] Perez, P.; Domingo, L. R.; Duque-Noreña, M.; Chamorro, E. , A Condensed-to-Atom Nucleophilicity Index. An Application to the Director Effects on the Electrophilic Aromatic Substitutions. *J. Mol. Struct. (Theochem),* **2009**, *895*, 86.

[32] Contreras, R.; Fuentealba, P.; Galván, M.; Perez, P. A direct evaluation of regional Fukui functions in molecules. *Chem. Phys. Lett.*, **1999**, *304*, 405.

[33] Geerlings, P.; De Proft, F.; Langenaeker, W. Conceptual density functional theory. *Chem. Rev.*, **2003**, *103*, 1793.

[34] Ess, D. H.; Jones, G. O; Houk, K. N. Conceptual, qualitative, and quantitative theories of 1,3-dipolar and Diels-Alder cycloadditions used in synthesis. *Advanced Synthesis & Catalysis,* **2006**, *348*, 2337.

[35] Domingo, L. R.; Aurell, M. J.; Perez, P.; Contreras, R.; Quantitative characterization of the global electrophilicity power of common diene/dienophile pairs in Diels–Alder reactions. *Tetrahedron,* **2002**, *58*, 4417.

[36] Jaramillo, P.; Domingo, L. R.; Chamorro, E.; Perez, P. A further exploration of a nucleophilicity index based on the gas-phase ionization potentials. *J. Mol. Struct.: THEOCHEM*, **2008**, *865*, 68.

[37] Berski, S.; Andres, J.; Silvi, B.; Domingo, L. R. The joint use of catastrophe theory and electron localization function to characterize molecular mechanisms. A density functional study of the Diels-Alder reaction. *J. Phys. Chem. A,* **2003**, *107*, 6014.

[38] Polo,V.; Andres, J.; Castillo, R.; Berski, S.; Silvi, B. Understanding the molecular mechanism of the 1,3-dipolar cycloaddition between fulminic acid and acetylene in terms of the electron localization function and catastrophe theory. *Chem. Eur. J.*, **2004**, *10*, 5165.

[39] Domingo, L. R.; Picher, M. T.; Arroyo, P.; Saez, J. A. 1,3-Dipolar cycloadditions of electrophilically activated benzonitrile *N*-oxides. Polar cycloaddition versus oxime formation. *J. Org. Chem.*, **2006**, *71*, 9319.

[40] Berski, S.; Andres, J.; Silvi, B., Domingo, L. R. New findings on the Diels-Alder reactions. An analysis based on the bonding evolution theory. *J. Phys. Chem. A,* **2006**, *110*, 13939.

[41] Polo, V.; Andres, J.; Berski, S.; Domingo, L. R.; Silvi, B. Understanding reaction mechanisms in organic chemistry from catastrophe theory applied to the electron localization function topology. *J. Phys. Chem. A*, **2008**, *112*, 7128.

[42] Domingo, L. R.; Chamorro, E.; Perez, P. Understanding the high reactivity of the azomethine ylides in [3+2] cycloaddition reactions. *Lett Org. Chem.*, **2010**, *7*, 432.

[43] Domingo, L. R.; Saez, J. A. Understanding the electronic reorganization along the nonpolar [3+2] cycloaddition reactions of carbonyl ylides. *J. Org. Chem.*, **2011**, *76*, 373.

[44] Domingo, L. R.; Aurell, M. J.; Perez, P.; Saez, J. A. Understanding the origin of the asynchronicity in bond-formation in polar cycloaddition reactions. A DFT study of the 1,3-dipolar cycloaddition reaction of carbonyl ylides with 1,2-benzoquinones. *RSC Adv.*, **2012**, *2*, 1334.

Caption to Figures

Figure 1. Schematic representation of disynaptic and monosynaptic basins [6] along synchronous bond formation in the N-DA reaction between Cp **1** and ethylene **2**.

Figure 2. Schematic representation of relevant disynaptic and monosynaptic basins [6] along the asynchronous bond formation in the P-DA reaction between Cp **1** and DCE **4**.

Figure 3. B3LYP/6-31G* geometries, relative energies and CT of the *endo* regiosiomeric TSs associated with the HDA reaction between nitroethylene **6** and DMVA **9**.

Figure 4. Schematic representation of disynaptic and monosynaptic basins along the ten phases characterizing the HDA reaction between nitroethylene **6** and DMVA **9**, represented by full lines and by ellipses with a dot, respectively. Dotted over full lines indicate a large basin population, while dotted lines indicate a low basin population. Filled ellipses indicate a very large basin population.

Figure 5. ELF attractors for selected points of the IRC from **TSno** to reagents and to **CAno**. Distances d1(C1-C6) and d2(O4-C7) are given in Angstroms.

Figure 6. Atomic spin densities of the anion radical of nitroethylene **6** and of the radical cation of DMVA **9**.

Figure 7. Plot of the relative activation energies of the *endo* TSs ($\Delta\Delta E_{(TSm-TSo)}$, in kcal/mol) *versus* (a) the CT (in e) and (b) the nucleophilicity N index (in eV).

Figure 8. Schematic representation of the most relevant phases involved in the C1-C6 and O4–C7 bond formation in the two-stages one-step mechanism of the HDA reaction between nitroethylene **6** and DMVA **9**. The CT and its direction (bold arrow) are represented in blue, while the C-to-C and O-to-C coupling between *pseudoradical* centers are given single-headed light green arrows.

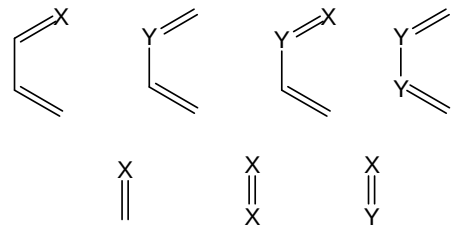

X = O, S, NH, PH ...
Y = N, P, ...

Some reagents involved in hetero-Diels-Alder reactions

Chart 1

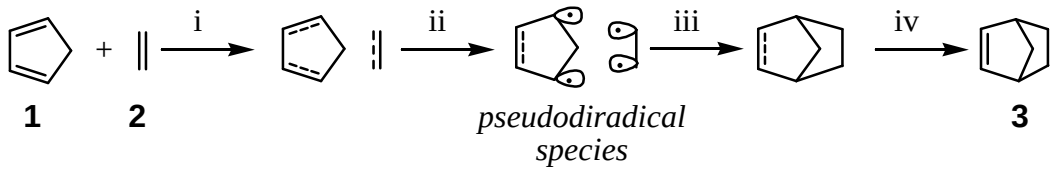

Figure 1. A schematic representation of disynaptic and monosynaptic basins [6] along synchronous bond formation in the N-DA reaction between Cp **1** and ethylene **2**.

.

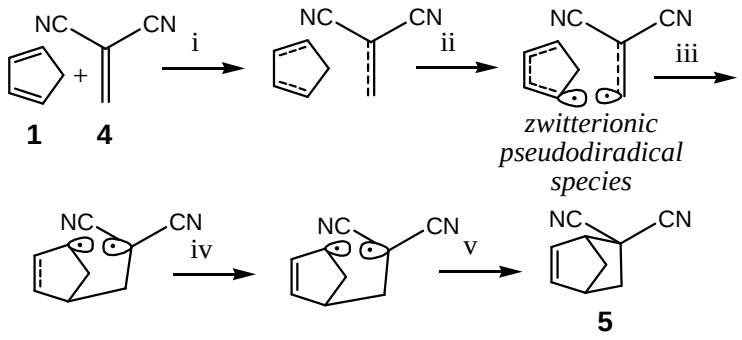

Figure 2. A schematic representation of relevant disynaptic and monosynaptic basins [6] along the asynchronous bond formation in the P-DA reaction between Cp **1** and DCE **4**.

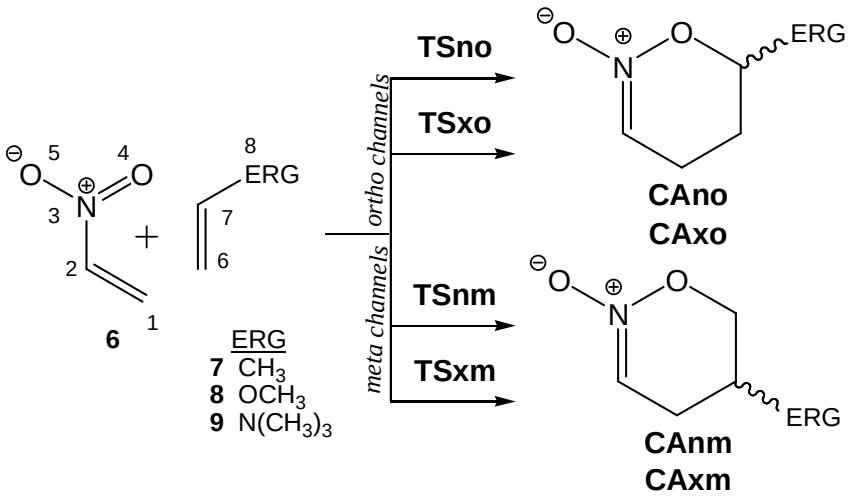
TSno
TSxo
TSnm
TSxm
ortho channels
meta channels
ERG
CAno
CAxo
CAnm
CAxm
6
ERG
7 CH3
8 OCH3
9 N(CH3)3

Scheme 1

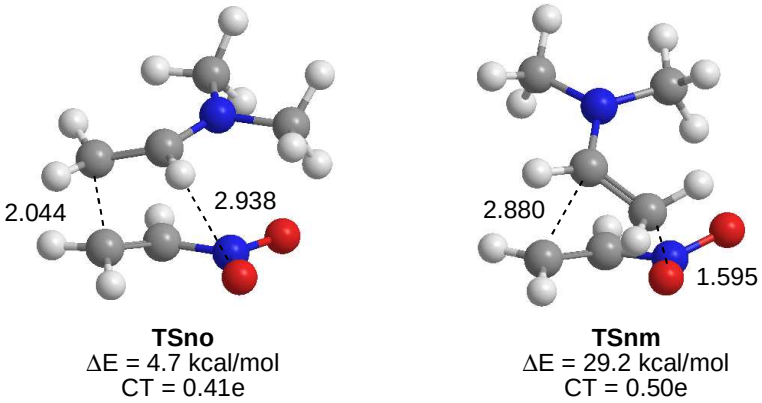

TSno
ΔE = 4.7 kcal/mol
CT = 0.41e

TSnm
ΔE = 29.2 kcal/mol
CT = 0.50e

Figure 3. B3LYP/6-31G* geometries, relative energies and CT of the *endo* regiosiomeric TSs associated with the HDA reaction between nitroethylene **6** and DMVA **9**.

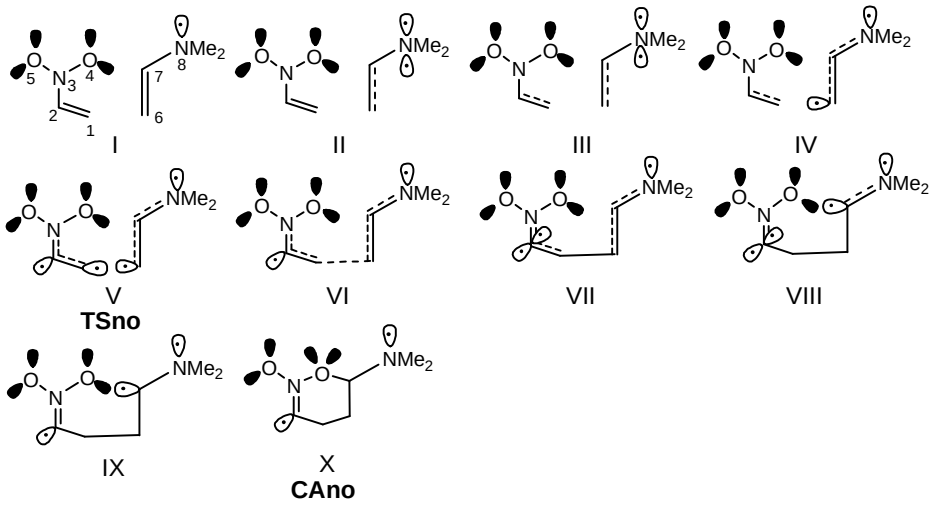

Figure 4. A schematic representation of disynaptic and monosynaptic basins along the ten phases characterizing the HDA reaction between nitroethylene **6** and DMVA **9**, represented by full lines and by ellipses with a dot, respectively. Dotted over full lines indicate a large basin population, while dotted lines indicate a low basin population. Filled ellipses indicate a very large basin population.

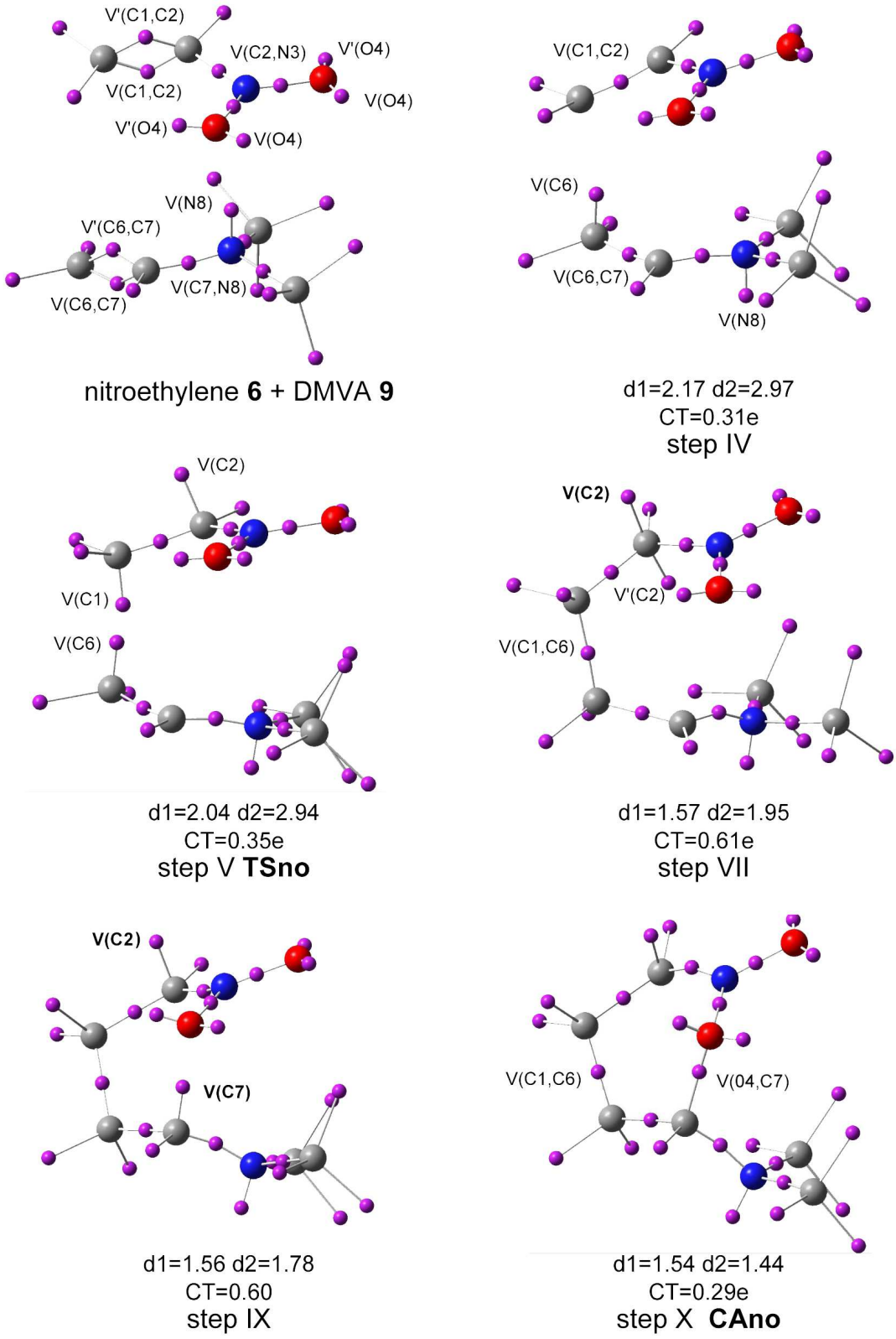

Figure 5. ELF attractors at selected points of the IRC from **TSno** to reagents and to **CAno**. The d1(C1,C6) and d2(O4,C7) distances are given in Angstroms.

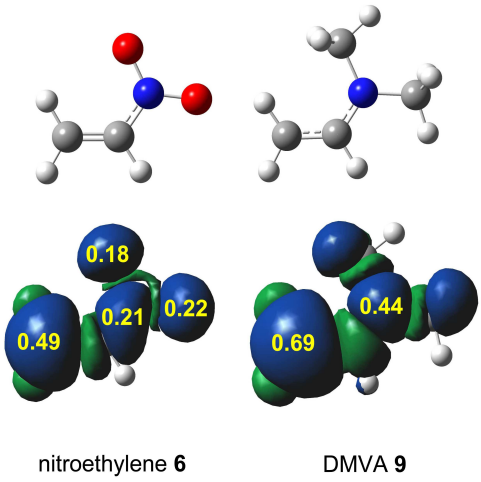

Figure 6. Atomic spin densities of the anion radical of nitroethylene **6** and of the radical cation of DMVA **9**.

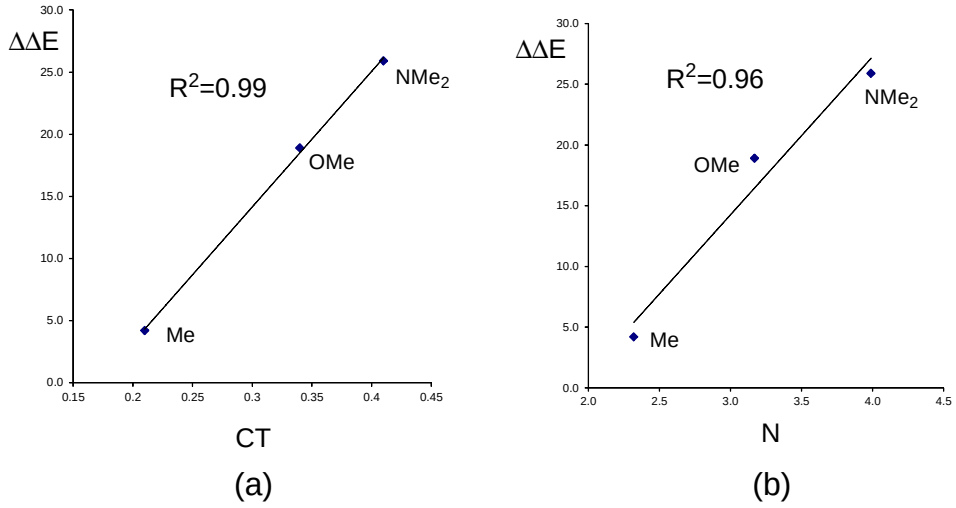

Figure 7. Plot of the relative activation energies of the *endo* TSs ($\Delta\Delta E_{(TSm-TSo)}$, in kcal/mol) *versus* (a) the CT (in e) and (b) the nucleophilicity N index (in eV).

.

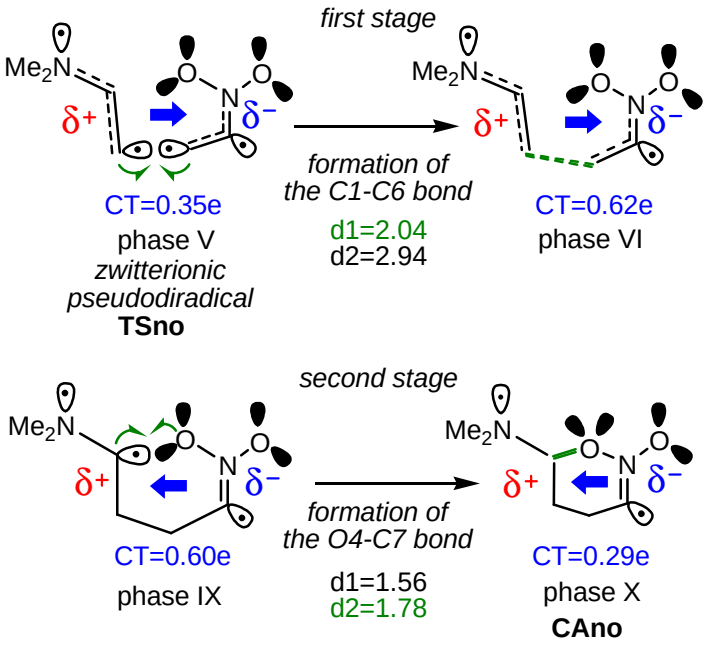

Figure 8. Schematic representation of the most relevant phases involved in the C1-C6 and O4–C7 bond formation in the two-stages one-step mechanism of the HDA reaction between nitroethylene **6** and DMVA **9**. The CT and its direction (bold arrow) are represented in blue, while the C-to-C and O-to-C coupling between *pseudoradical* centers are given single-headed light green arrows.